ADVANCED MATERIALS

Supporting Information

for *Adv. Mater.,* DOI: 10.1002/adma.202200902

Toward Plasmonic Neural Probes: SERS Detection of Neurotransmitters through Gold-Nanoislands-Decorated Tapered Optical Fibers with Sub-10 nm Gaps

Di Zheng, Filippo Pisano, Liam Collard, Antonio Balena, Marco Pisanello, Barbara Spagnolo, Rosa Mach-Batlle, Francesco Tantussi, Luigi Carbone, Francesco De Angelis, Manuel Valiente, Liset M. de la Prida, Cristian Ciracì, Massimo De Vittorio,* and Ferruccio Pisanello**

Supporting information for

Toward plasmonic neural probes: SERS detection of neurotransmitters through gold nanoislands-decorated tapered optical fibers with sub-10 nm gaps

*Di Zheng[1, *], Filippo Pisano[1], Liam Collard[1], Antonio Balena[1], Marco Pisanello[1], Barbara Spagnolo[1], Rosa Mach-Batlle[1], Francesco Tantussi[2], Luigi Carbone[3], Francesco De Angelis[2], Manuel Valiente[4], Liset de La Prida[5], Cristian Ciracì[1], Massimo De Vittorio[1,6, *, †], Ferruccio Pisanello[1, *, †]*

[1] *Istituto Italiano di Tecnologia, Center for Biomolecular Nanotechnologies, Arnesano, LE 73010, Italy*

[2] *Istituto Italiano di Tecnologia, Center for Convergent Technologies, Genova, 16163, Italy*

[3] *CNR NANOTEC, Institute of Nanotechnology, Lecce, 73100, Italy*

[4] *Brain Metastasis Group, Spanish National Cancer Research Center (CNIO), Madrid, 28029, Spain*

[5] *Instituto Cajal, CSIC, Madrid, 28002 Spain*

[6] *Dipartimento di Ingegneria Dell'Innovazione, Università del Salento, Lecce 73100, Italy*

**Authors to whom correspondence should be addressed: di.zheng@iit.it, massimo.devittorio@iit.it, Ferruccio.pisanello@iit.it*

† *These authors contributed equally to this work*

- **Section S1 LOD experiment for blank TF**

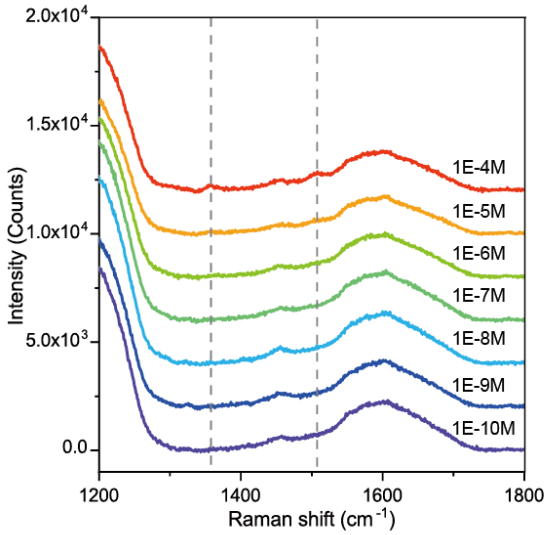

Figure S1 *Blank TF detects R6G in aqueous solution with different concentrations, from the bottom to the top, the concentration varies from* 10^{-10} *M to* 10^{-4}*M, the spectra were offset vertically for easier visualization. The R6G molecule peaks of 1356* cm^{-1} *and 1504* cm^{-1} *start to appear at a concentration of* 10^{-4} *M.*

- **Section S2 Reproducibly and repeatability of NIs-TFs fabrication**

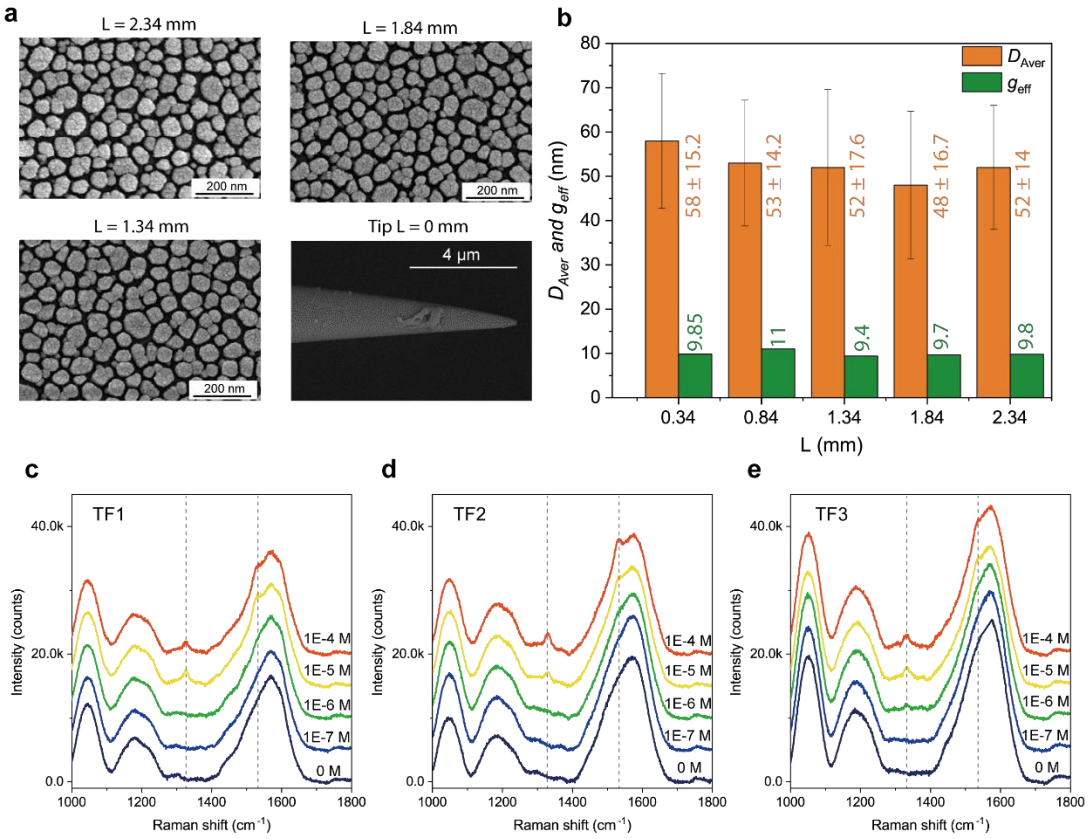

Figure S2.1 *(a) High magnification SEM images for the statistical analysis (the notes on the top of each image indicate the positions on the fiber). (b) Statistical analysis for average NIs diameter (orange bars) and effective gap size (green bars) distribution starting from the very tip L = 0.34 mm to the taper end of L = 2.34 mm. (c-e) Reproducibility and repeatability test for three npRDW TFs detecting serotonin water solutions with different concentrations (the solid curves), the spectra were offset vertically for easier visualization, and the vertical dashed lines indicate the serotonin molecule peaks at 1335 cm^{-1}, 1535 cm^{-1}.*

We fabricated multiple batches of npRDW TFs with the same film deposition parameters and dewetting conditions to check the reproducibility of the probes and repeatability of the LOD. SEM inspections revealed that the different probes have similar morphologies with similar particle average diameters and effective gap sizes; a representative set of images is reported in **Fig.S2.1a**, with the quantitative analysis displayed in **Fig.S2.1b**. Serotonin was chosen as analyte to conduct the repeatability LOD experiment. **Fig.S2.1c-e** reports reproducibility data for serotonin LOD from three different fibers randomly selected from the same batch. It shows that serotonin molecule peaks at 1335 cm^{-1} and 1535 cm^{-1} become prominent from a concentration of 10^{-5} M for TF1 and TF2, while TF3 also show a recognizable signature peak at 1335 cm^{-1} from a concentration of 10^{-6} M.

- **Section S3 NIs morphology statistical analysis**

In **Fig.S3.1** we show histograms of NIs diameter (obtained by circular approximation

of each NIs occupation area) extracted from npSDW and npRDW NIs-TFs SEM morphologies. The first row corresponds to npSDW TF, and the second row corresponds to npRDW TF. The histograms are arranged from the tip region to the taper end (from left to right) with the corresponding curvatures of the TF positions marked on the top of each histogram, along with corresponding SEM images shown in the inset. It can be clearly seen from the histograms that due to the bimodal distribution of twice successive dewetting process, the npRDW NIs-TF has a wider size distribution at every curvature than the npSDW NIs-TF. Thus, the effective gap size evaluation that depends on circular and one-modal periodic approximation can be less representative for RDW bimodal distribution cases.

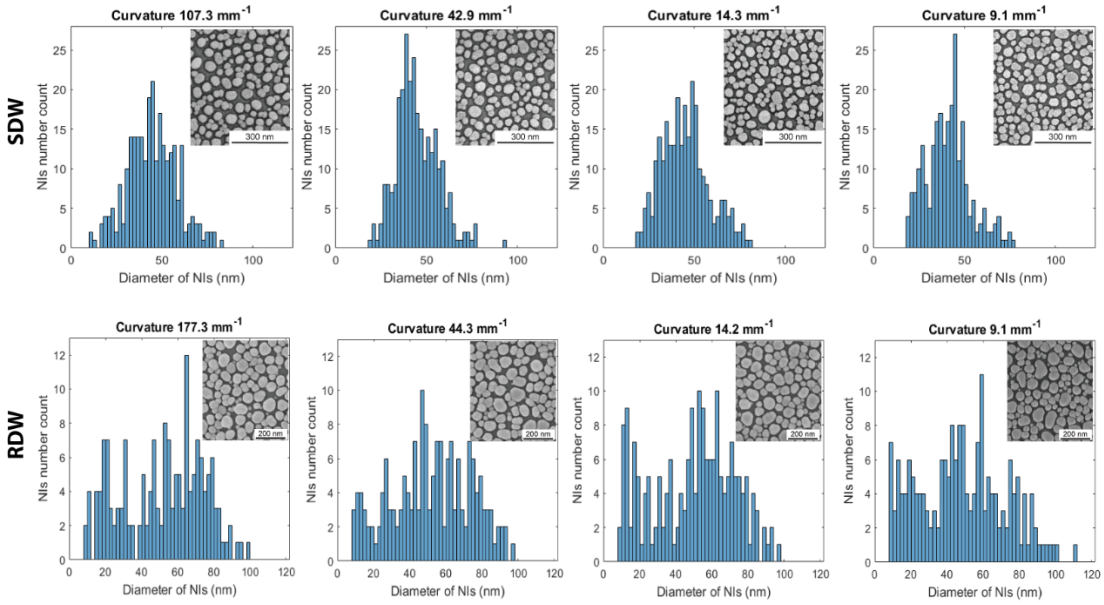

Figure S3.1 *The histograms of NIs' diameter distributions for npSDW (first row) and npRDW (second row) NIs-TFs. Figures from left to right are the histograms correspond to very tip regions to taper end with the curvatures of the TF positions marked at the top of each figure.*

Thus, we developed a more generalized computational method to analyses the effective gap size of NIs without introducing any circular and periodic approximation. The method relies on finding the minimal distances between each NI to its' nearest neighbor by point-to-point computation of the NIs boundaries, and the effective gap is defined by averaging all the minimal distances that has been found. Here, we use the computation method to analysis the bimodal distributed RDW morphology in **Fig.3a**. The representative analyzing result is shown in **Fig.S3.2a**, where the NIs' boundaries (blue circles) and the minimal distances (red lines) have been overlayed with the original SEM images. The histogram in **Fig.S3.2b** shows the distribution of the minimal distances, with the effective gap size determined by the average number of 8.6 nm, and the standard deviation is 2.9 nm.

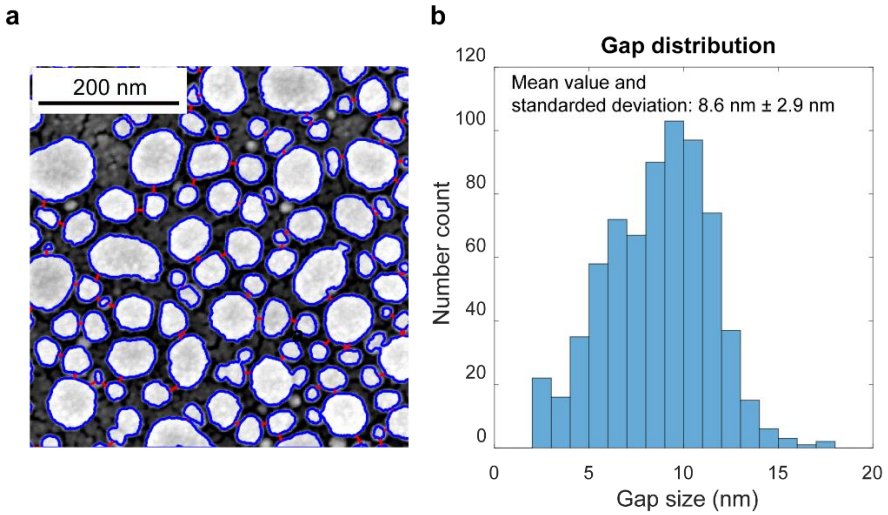

Figure S3.2 *(a) The boundaries (blue circles) and the minimal distances (red lines) overlay with the RDW SEM images. (b) The histogram of the minimal distances that has been found by computational method.*

To compare the difference between the generalized computational method to the method used in the manuscript, we analyzed the same set of data in **Fig.2d** with the generalized computational method. The results were plotted in the bar graph (**Fig.S3.3**) with average diameters (obtain with circular approximation from occupation area) and effective gaps. It showed that the effective gaps have an slightly decreased value, and the distribution along the fiber have the same stable appearance as the results in **Fig.2d.**

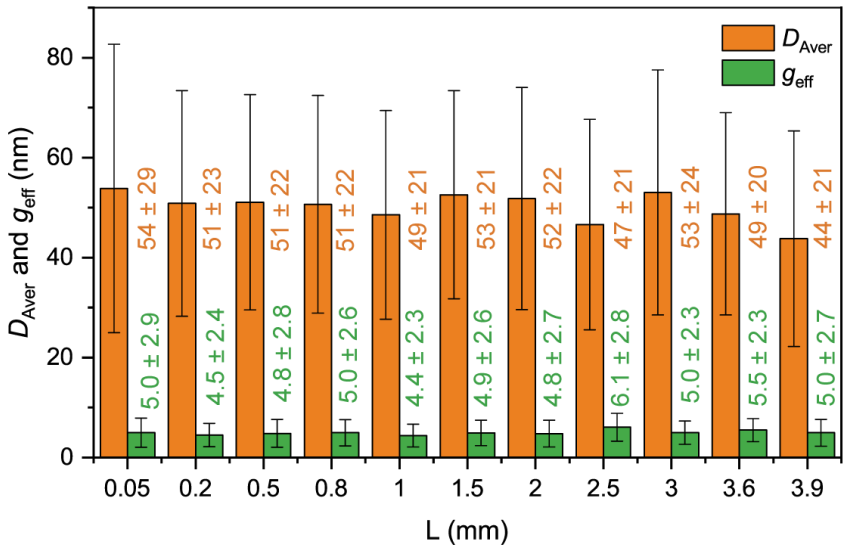

Figure S3.3 *Use the generalized computational method to analyze the npRDW morphology data along the TF in Fig.2d.*

- **Section S4 The electromagnetic properties of gold NIs and silica TF**

The geometric parameters for the plasmonic structures distributed on the TF play an

important role for the device performance. The solid-state dewetted NIs is very thin, the thickness can be estimated around 15 nm to 20 nm (derived from T/C, where T = 10 nm is the total nominal film thickness during fabrication, and C is the coverage rate, ranging between 50% to 64% from different batches for RDW). The hexagonal period model with representative parameters obtained experimentally show when the in-plane mode has been generated, the near-field enhancement is mainly in gaps, and very close to the interface (from the cross section) in **Fig.S4.1a**, the resonances stay unchanged with two different polarizations (**Fig.S4.1b**). Detailed studies also show the plasmonic resonance of the solid-state dewetted NIs are insensitive to the rotation angle of p-polarized light (electric field polarized parallel to the plane of incidence), and is insensitive to the incidence angle[1].

Thus, dewetted NIs have advantages when coupling with the electromagnetic field on the TF (**Fig.S4.2**), when radiative mode and guide mode (generate wide extended evanescence field on the wide taper surface) both exist at taper region. When the very thin NIs locates directly on the taper surface, it interacts with radiative mode, and maximizes the coupling with the evanescence field, which only extend hundreds of nanometers to the environment from fiber surface (only 233 nm in water at the very tip region with diameter of 1 um shown in **Fig.S4.2e**), facilitating the generation and the collection of inelastic scattered SERS signal. The efficient coupling of plasmonic structures extends optically sensitive region on taper and the coupling region is recognizable from far-field scattering when send light into the fiber through a fiber patch cord (**Fig.S4.3**).

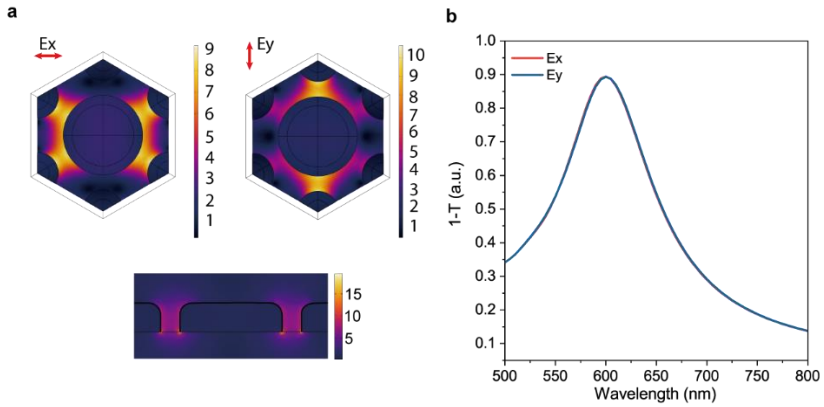

Figure S4.1 *(a) In plane near-field distributions for hexagonal periodic model under Ex and Ey excitations (the diameter of central and surrounding gold disks are 53 nm and 28 nm respectively; the gap is 10 nm, and the thickness of the disks is 15 nm). The bottom is the cross section along the central axis under Ey excitation. (b) The spectra response of hexagonal periodic model under Ex and Ey excitation, reported with a coefficient (1 - T), where T is the transmittance of the system at normal incidence.*

Fig.4.2a is the schematic illustration for the longitudinal cross-section geometry of the tapered fiber, where both core (refractive index 1.464) and cladding (refractive index 1.447) are narrowing along fiber length. The relationship between R1 (radius of core) and R2 (radius of core and cladding) are given by $R2 = 1.1 \times R1$.

To understand the light propagation and distribution along the taper, we have calculated the modes at a given transverse cross-section diameter of 1 μm using the eigenmode solver in COMSOL Multiphysics. The waveguide cross-section is simulated in the water environment (refractive index 1.33) with the excitation wavelength of 785 nm. In **Fig.4.2b** and **c**, the radiative mode has an effective mode index of 1.33, and the guided mode has an effective mode index of 1.4003 (note that this is smaller than the cladding refractive index since the mode extends out of the cladding into the water environment). The field distribution profiles of the radiative mode and guided mode (marked with red and blue dashed line in **Fig.S4.2b** and **c**) are show in **Fig.4.2d**. The evanescent tail of guided mode is fitted with exponential decay model in **Fig.S4.2e**, which gives a decay length of 233 nm.

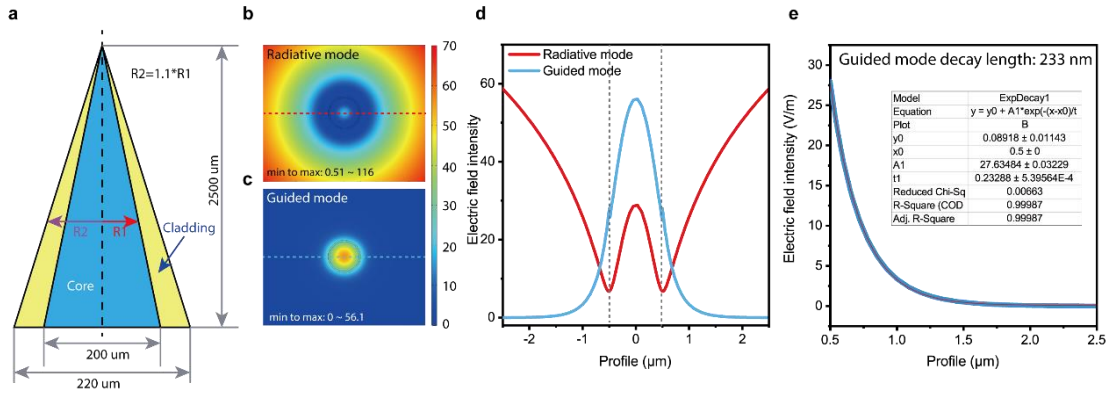

Figure S4.2 *(a) Sketch of the TF geometry. (b) and (c) are the simulated electromagnetic fields distribution of transverse cross-section for radiative mode and guided mode when fiber is immersed in water, the fiber cross section diameter is 1 μm, the excitation wavelength is 785 nm, and the refractive indexes for the core and cladding are 1.464 and 1.447. (d) The profile of field distribution extracted from radiative mode (red line) and the guided mode (blue line) along the central axis. (e) The evanescent tail of the guided mode extends from the cladding surface to the water environment, and the exponential fitting show the decay length is 233 nm.*

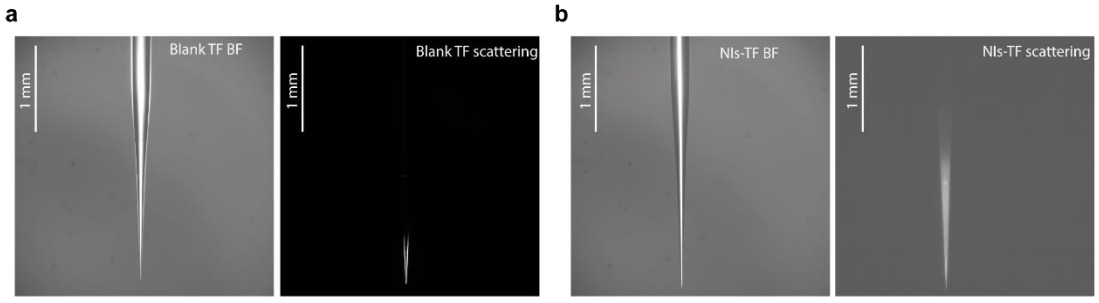

Figure S4.3 *The scattering images of blank TF (a) and NIs-TF (b). The scattering light along the NIs-TFs is nearly 3 times longer in length with respect to blank TF. The halogen excitation light was sent through the fiber patch cord to deliver light to TF, and the TFs (NA = 0.22) were put horizontally under microscope with a 4X objective (NA = 0.28).*

- **Section S5 Optical measurement setups**

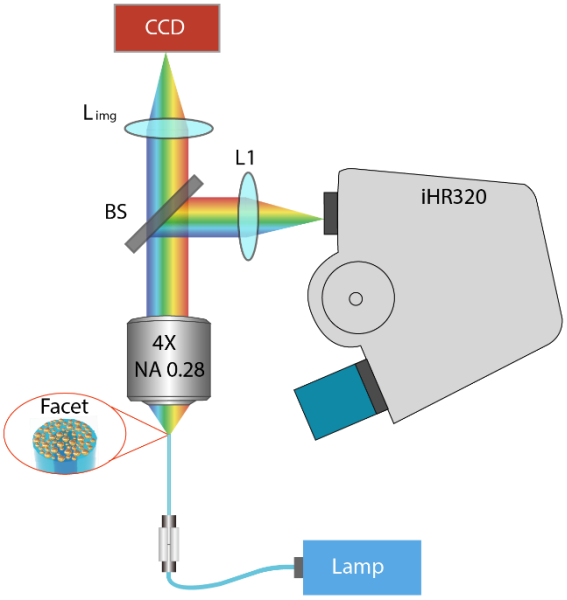

Figure S5.1 *The optical setup for extinction spectra measurement. L1 (lens with f = 100 mm), L2 (Thorlabs TTL200 tube lens f_{img} = 200 mm), BS (beam splitter T : R = 50 : 50), CCD (sCMOS camera, Orca Fusion, Hamamatsu), Lamp (Mikropack, HL-2000-FHSA).*

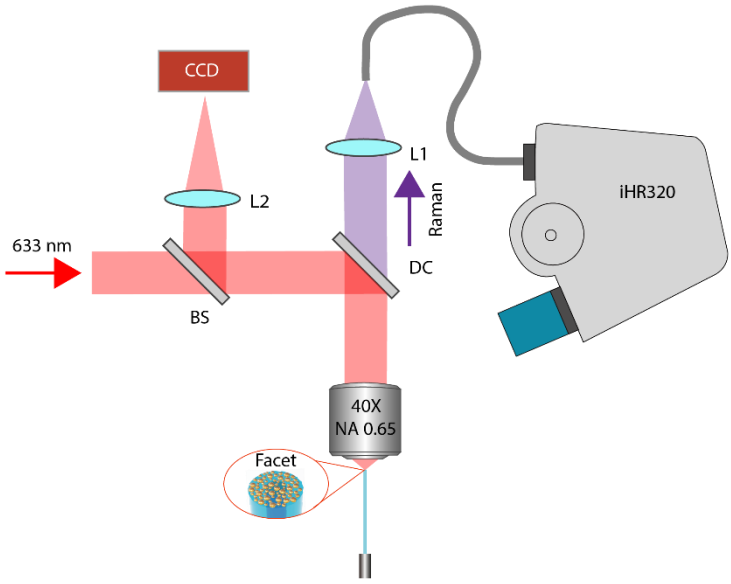

Figure S5.2 *The optical setup for Raman measurements at 633 nm. DC (dichroic mirror, Semrock, LPD02-633RU), L1 (lens with f = 50 mm), L2 (lens with f = 100 mm), BS (beam splitter with T : R = 90 : 10), CCD (Thorlabs CMOS camera, DCC1545M).*

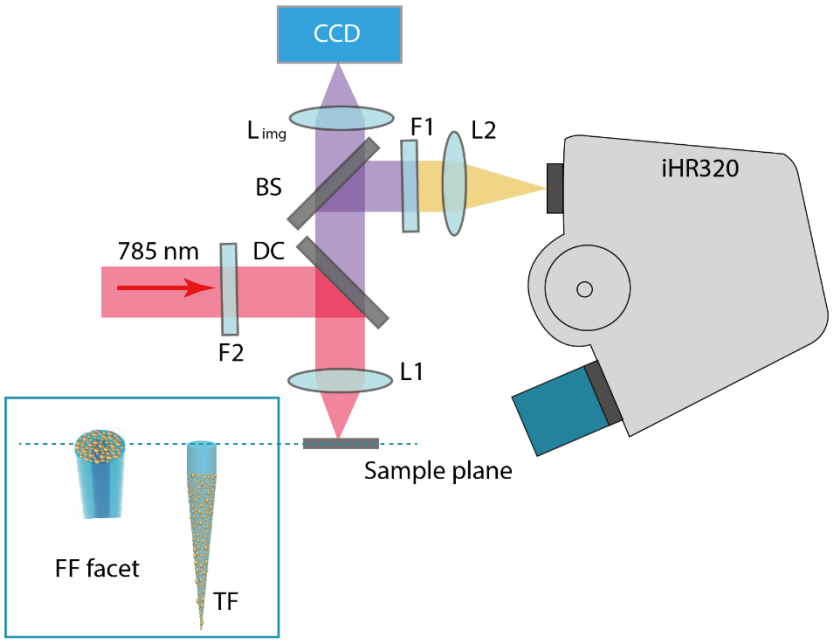

Figure S5.3 *The optical setup for Raman measurements with different sample configurations at 785 nm. DC (dichroic mirror, Semrock, LPD02-785RU-25), focus lens L1 (aspheric Ø25.0 mm, f = 20 mm), collection lens L2 (Thorlabs, TTL200MP, f = 200 mm), image lens L_{img} (Thorlabs, WFA4100), F1 (long pass filter, Semrock, LP02-785RU-25), F2 (laser line filter, Semrock, LL01-785-25), BS (beam splitter with T : R = 50 : 50), CCD (Thorlabs CMOS camera, DCC1545M).*

[1] G. Gupta, D. Tanaka, Y. Ito, D. Shibata, M. Shimojo, K. Furuya, K. Mitsui, K. Kajikawa, *Nanotechnology* **2009**, *20*, 025703.